JOURNAL OF VIROLOGY, June 2010, p. 6188–6199 Vol. 84, No. 12
0022-538X/10/$12.00 doi:10.1128/JVI.02420-09

Structure of Foot-and-Mouth Disease Virus Mutant Polymerases with Reduced Sensitivity to Ribavirin▽†

Cristina Ferrer-Orta,[1] Macarena Sierra,[2] Rubén Agudo,[2] Ignacio de la Higuera,[2] Armando Arias,[2] Rosa Pérez-Luque,[1] Cristina Escarmís,[2] Esteban Domingo,[2,3] and Nuria Verdaguer[1]*

Institut de Biologia Molecular de Barcelona (CSIC), Parc Científic de Barcelona, E-08028 Barcelona, Spain[1]; Centro de Biologia Molecular Severo Ochoa (CSIC-UAM), Cantoblanco, E-28049 Madrid, Spain[2]; and Centro de Investigación Biomédica en Red de Enfermedades Hepáticas y Digestivas (CIBERehd), Barcelona, Spain[3]

Received 17 November 2009/Accepted 4 April 2010

Passage of poliovirus (PV) or foot-and-mouth disease virus (FMDV) in the presence of ribavirin (R) selected for viruses with decreased sensitivity to R, which included different mutations in their polymerase (3D): G64S located in the finger subdomain in the case of PV and M296I located within loop β9-α11 at the active site in the case of FMDV. To investigate why disparate substitutions were selected in two closely related 3Ds, we constructed FMDVs with a 3D that included either G62S (the equivalent replacement in FMDV of PV G64S), M296I, or both substitutions. G62S, but not M296I, inflicts upon FMDV a strong selective disadvantage which is partially compensated for by the substitution M296I. The corresponding mutant polymerases, 3D(G62S), 3D(M296I), and 3D(G62S-M296I), were analyzed functionally and structurally. G62S in 3D impairs RNA-binding, polymerization, and R monophosphate incorporation activities. The X-ray structures of the 3D(G62S)-RNA, 3D(M296I)-RNA, and 3D(G62S-M296I)-RNA complexes show that although the two positions are separated by 13.1 Å, the loops where the replacements reside are tightly connected through an extensive network of interactions that reach the polymerase active site. In particular, G62S seems to restrict the flexibility of loop β9-α11 and, as a consequence, the flexibility of the active site and its ability to bind the RNA template. Thus, a localized change in the finger subdomain of 3D may affect the catalytic domain. The results provide a structural interpretation of why different amino acid substitutions were selected to confer R resistance in closely related viruses and reveal a complex network of intra-3D interactions that can affect the recognition of both the RNA template and incoming nucleotide.

Ribavirin (1-β-D-ribofuranosyl-1-*H*-1,2,4-triazole-3-carboxamide) (R) is a clinically important nucleoside analogue that exhibits antiviral activity against a broad spectrum of RNA viruses (17). R displays several antiviral mechanisms of action, including lethal mutagenesis (loss of infectivity associated with an increase in the mutation rate) (7, 9, 21, 23). The 5′-triphosphorylated form of R (RTP) can be incorporated by the viral polymerases into the nascent RNA, acting as either an adenylate or a guanylate analogue, inducing base transitions. Ambiguous utilization of RTP by RNA-dependent RNA polymerases during genome replication may lead to virus extinction (1, 6, 7, 33).

As extensively documented for nonmutagenic antiviral inhibitors, selection of mutagen-resistant viruses may be a problem for the efficacy of antiviral treatments based on lethal mutagenesis. Serial passages of foot-and-mouth disease virus (FMDV) in the presence of increasing concentrations of R resulted in the selection of a mutant virus containing the amino acid substitution M296I in polymerase 3D. Measurements of viral fitness and progeny production suggested that M296I was selected because it decreased the mutagenic activity of R on FMDV (28). The mutant polymerase restricted the incorporation of RTP during RNA synthesis, relative to the wild-type enzyme, without an increase in average copying fidelity. Rather, the mutant enzyme displayed an about 2-fold lower RTP incorporation frequency and an about 2.5-fold increase in the A-to-G transition frequency (3). The substitution M296I in 3D conferred upon FMDV resistance to extinction by high R concentrations, but extinction of the mutant was achieved by an alternative mutagenic treatment (22).

In contrast to passage of FMDV, passage of poliovirus (PV) in the presence of R selected a mutant virus that included the replacement G64S in 3D (25). This substitution conferred upon 3D a higher average copying fidelity, allowing the enzyme to restrict the incorporation of RTP in the place of ATP or GTP (4, 6). The increased copying fidelity gave rise to PV populations that were less adaptable than wild-type populations to a complex environment, represented by PV-susceptible mice (24, 32). In FMDV 3D, the substitution equivalent to G64S in PV is G62S. This replacement was never selected in FMDV passaged in the presence of R and was never detected as a minority component in mutant spectra of FMDV that replicated in the absence or presence of R or other mutagenic agents (1, 28, 29).

To interpret the selection of disparate R resistance mutations in FMDV and PV and to gain insight into the molecular basis of R resistance, we have engineered FMDVs encoding

* Corresponding author. Mailing address: Institut de Biología Molecular de Barcelona (CSIC), Parc Cientific de Barcelona, Baldiri i Reixac 10, E-08028 Barcelona, Spain. Phone: 34 93 403 49 52. Fax: 34 93 403 49 79. E-mail: nvmcri@ibmb.csic.es.

† Supplemental material for this article may be found at http://jvi.asm.org/.

▽ Published ahead of print on 14 April 2010.

3D with G62S, alone and together with M296I and compared the behavior of the mutants with that of wild-type FMDV. We have purified the corresponding 3Ds with the G62S, the M296I, or both substitutions and determined their polymerase activities and three-dimensional structures alone and in several catalytic complexes. The results show that FMDV expressing 3D with G62S is genetically unstable and that the reason for its instability probably lies in impaired polymerase activity associated with the conformation acquired by a loop located close to motif B (loop β9-α11, residues 294 to 304) which is involved in interactions with the template RNA and with the incoming nucleotide. Comparison of the structures revealed that the mutated residues, G62S and M296I, are involved in an extensive network of interactions that affect residues directly required for the catalytic function of the enzyme.

MATERIALS AND METHODS

Cells, viruses, and infections. The origin of the BHK-21 cells used and the procedures used for cell growth and infection with FMDV in the presence or absence of R have been previously described (1, 28, 30). FMDV C-S8c1 is a plaque-purified derivative of natural isolate C1 Santa-Pau Spain 70 (30), a representative of European serotype C FMDV.

Preparation of FMDV C-S8c1 with substitutions in 3D. Plasmid pMT28 encodes an infections transcript of FMDV C-S8c1 (15). A pMT28 derivative encoding FMDV C-S8c1 with the substitution M296I in 3D [termed pMT28-3D(M296I)] was constructed by site-directed mutagenesis of codon 296 of 3D. Two PCR amplifications encoding the replacement M296I were obtained with two different pairs of primers. The amplicons were shuffled, and the resulting DNA was digested and ligated to linearized pMT28 as previously described (28). To produce pMT28 with the substitution G62S in 3D [termed pMT28-3D(G62S)], GGA codon 62 of 3D was changed to TCA. The two pairs of primers used to obtain mutagenic DNA amplifications were 3AR3 (GATGACGTGAA CTCTGAGCCCGC; sense, 5′ position 5710)-GS2 minus (AGACATCTTTGT GTCT**GA**TTATGCTTGGAGAAAATGAC; antisense, 5′ position 6810) and GS2S plus (TCATTTTCTCCAAGCATAAA**TC**AGACACAAAGATGTCTG CGG; sense, 5′ position 6772)-AV3 (TTCATGGCATCGCTGCAGTGG; antisense, 5′ position 7370) (residue numbering is according to reference 12; boldface letters indicate modifications of the genomic sequence to introduce the replacement G62S). Shuffling of the two amplicons, restriction enzyme digestion, and ligation to linearized pMT28 were carried out as previously described (28). The preparation of pMT28 with the substitutions G62S and M296I in 3D [termed pMT28-3D(G62S-M296I)] was carried out as described for pMT28-3D(G62S), except that the parental plasmid was pMT28-3D(M296I) instead of pMT28. In all constructs, the presence of the desired mutations was ascertained by nucleotide sequencing of the 3D coding region.

Infectious transcripts were prepared as previously described (28). Concentrations of the RNA transcripts were estimated by agarose gel electrophoresis and ethidium bromide staining, with known amounts of *Escherichia coli* rRNA as the standard. About 1 μg of RNA transcript was transfected into BHK-21 cells using Lipofectin (Gibco), and cells were cultured until cytopathology was complete. The virus obtained was passaged in BHK-21 cells using the standard infection protocol, and the number of passages is indicated for each experiment. Samples of virus obtained in the initial transfection and from subsequent passages were stored at −70°C for further study.

Molecular cloning, expression, and purification of FMDV 3D. FMDV 3D with the substitution G62S or M296I or both G62S and M296I [termed 3D(G62S), 3D(M296I), and 3D(G62S-M296I), respectively] were obtained by site-directed mutagenesis from plasmid pET-28a3Dpol (pET-28a [Novagen] containing the FMDV polymerase 3D coding region [2]) using the QuikChange site-directed mutagenesis kit (Stratagene) as previously described (3). Mutant 3Ds were expressed and purified by affinity chromatography as previously described (14); the enzymes were >95% pure, as judged by sodium dodecyl sulfate-polyacrylamide gel electrophoresis and Coomassie brilliant blue staining.

Polymerization assays with 3Ds. Specific activity of mutant 3Ds was determined by measuring the incorporation of UMP directed by the homopolymeric poly(A)/oligo$(dT)_{15}$ template-primer. The standard reaction mixture included 30 mM morpholinepropanesulfonic acid (MOPS, pH 7.0), 33 mM NaCl, 5 mM $Mg(CH_3COO)_2$, 40 ng/μl poly(A) (average of 300 residues; Amersham Pharmacia), 2.36 μM oligo$(dT)_{15}$ (Life Technologies), 500 μM [α-^{32}P]UTP (0.01 mCi/ml; 20 mCi/mmol; Perkin-Elmer), and 0.4 to 0.8 μM 3D. A mixture (46 μl) of all of the components except 3D was prewarmed at 37°C for 2 min, and the reaction was started by adding 4 μl of 3D (in 50 mM Tris-HCl [pH 7.5]–100 mM NaCl–1 mM EDTA–10% [vol/vol] glycerol). The reaction was carried out for 5 min at 37°C and stopped by adding 10 μl of 500 mM EDTA. The reaction mixture was spotted onto a DE81 filter (Whatman). To remove the UTP that was not incorporated, the filter was washed three times with an excess of 0.2 M Na_2HPO_4 and then rinsed in ethanol and dried for 15 min at 55°C. The radioactivity was measured by PhosphorImager analysis (BAS-1500; Fuji).

To measure incorporation of RTP by wild-type and mutant 3Ds, the heteropolymeric sym/sub template-primers (4) 5′-GUACGGGCCC-3′ (sym/sub-C) and 5′-GCAUGGGCCC-3′ (sym/sub-U) (Dharmacon Research) were used. The oligonucleotides were purified, end labeled with [γ-^{32}P]ATP and polynucleotide kinase (NEB), and annealed using standard protocols (4). For the reaction with sym/sub-C, the latter and 3D (3 μM) were incubated in 30 mM MOPS (pH 7.0)–33 mM NaCl–15 mM $Mg(CH_3COO)_2$ for either 10 min [for 3D and 3D(M296I)] or 20 min [for 3D(G62S) and 3D(G62S-M296I)] at 37°C and then mixed with either 50 μM GTP or 50 μM RTP (final volume, 70 μl). At different times (0 to 40 min) after the addition of GTP or RTP, the reaction was stopped by the addition of EDTA (83 mM final concentration). The same procedure was followed with sym/sub-U, except that ATP was used as a substrate instead of GTP. Reaction products were analyzed by electrophoresis on a denaturing 23% polyacrylamide–7 M urea gel in 90 mM Tris base–90 mM boric acid–2 mM EDTA. The 10-mer and 11-mer (sym/sub elongated by one nucleotide) forms were visualized and quantitated with a PhosphorImager (BAS-1500; Fuji).

Gel mobility shift assays. The RNA-binding capacity of the mutant polymerases was studied by gel mobility shift assays as previously described (2). Briefly, an RNA sym/sub-U was labeled and annealed as described above for the polymerization assays. The reaction mixture included 100 mM MOPS (pH 7.0), 20 mM NaCl, 25 mM $MgCl_2$, 5% (wt/vol) polyethylene glycol, and 20 nM ^{32}P-labeled RNA sym/sub-U. The binding reaction was started with the addition of 3D. The mixture was incubated for 10 min at 37°C and then loaded onto a nondenaturing 10% polyacrylamide gel in TB buffer (85 mM Tris-HCl, 85 mM boric acid, pH 8.0) and subjected to electrophoresis at 100 V at 4°C for 1 h. The gel was fixed in 10% (vol/vol) ethanol–10% (vol/vol) acetic acid and dried for 45 min at 80°C. The proportion of sym/sub in complex with 3D was calculated as previously described (2).

Crystallization and soaking experiments. Purified FMDV mutant polymerases 3D(M296I), 3D(G62S), and 3D(G62S-M296I) were stored in a buffer containing Tris-HCl (40 mM, pH 7.5), NaCl (0.5 M), dithiothreitol (0.8 mM), EDTA (0.8 mM), and glycerol (8%) (crystallization buffer) at a concentration of 4.6 mg/ml. The 3D-RNA sym/sub-U binary complexes were obtained as previously described (13). To produce the 3D(M296I)-RNA-GTP ternary complex, the 3D(M296I)-RNA cocrystals were soaked for 6 h in a harvesting solution containing the crystallization buffer, 2 mM $MnCl_2$, and 2 mM GTP before flash-freezing in liquid nitrogen. Attempts to obtain additional ternary complexes from 3D(M296I)-RNA, 3D(G62S)-RNA, and 3D(G62S-M296I)-RNA with ATP or RTP were unsuccessful; the substrates were not incorporated into the crystals, even when high nucleotide concentrations (up to 25 mM) or long incubation times (a few days) were used.

Data collection, structure determination, and refinement. Four different data sets were collected at 100 K, 3D(M296I)-RNA (2.8 Å), 3D(M296I)-RNA-GTP (2.4 Å), 3D(G62S)-RNA (2.2 Å), and 3D(G62S-M296I)-RNA (2.1 Å), using synchrotron radiation at European Synchrotron Radiation Facility (ESRF) beamlines ID14 EH1 and EH2 (λ = 0.93 Å). All data were processed and reduced using the DENZO/SCALEPACK package (Table 1) (20).

The initial maps of the 3D(M296I)-RNA, 3D(G62S)-RNA, and 3D(G62SM296I)-RNA complexes ($P3_221$ crystals) were obtained after a rigid-body fitting of the coordinates of isolated 3D protein that was crystallized in the trigonal $P3_221$ space group (Protein Data Bank [PDB] code 1WNE) (14) to the new unit cells using the program REFMAC. Initial maps of 3D(M296I)-RNA-GTP and 3D(G62S)-RNA (tetragonal crystals) were obtained by following the same procedure but using the tetragonal $p4_22_12$ coordinates of 3D (PDB code 1U09) (14) as the starting model (Table 1). In the four structures, the 2|Fo|-|Fc| and |Fo|-|Fc| difference maps clearly allowed repositioning of the mutated residues and surrounding regions and showed the presence of extra densities corresponding to the RNA substrates. Several cycles of automatic refinement, performed with the program REFMAC, were alternated with manual model rebuilding using the graphic programs TURBO and Coot (11, 26). The statistics of the refinement for the four complexes are summarized in Table 1.

Coordinate accession numbers. The coordinates and structure factors for 3D, 3D(M296I), 3D(M296I)–GTP, 3D(G62S) $p3_221$, 3D(G62S) $p4_12_12$, and

TABLE 1. X-ray data collection and refinement statistics

Parameter	3D(G62S)[a]	3D(G62S)[b]	3D(M296I)[c]	3D(M296I)-GTP[d]	3D(G62SM296I)[e]
Resolution (Å)	20–2.2	20–2.1	20–2.8	30–2.4	20–2.6
Space group	$P3_221$	$P4_12_12$	$P4_12_12$	$P3_221$	$P3_221$
Unit cell dimensions (Å)	a = b = 93.9 c = 100.0	a = b = 93.7 c = 121.1	a = b = 93.6 c = 120.9	a = b = 95.4 c = 100.9	a = b = 93.7 c = 99.4
Total data	143,526	243,388	75,096	100,003	68,927
Unique data	26,125	59,922	13,868	16,713	15,634
Completeness (%)	99.1	98.7	99.9	99.9	98.2
Mean I/σ (Di)[f]	15.8	14.9	21.6	17.1	13.6
R_{merge} (%)[g]	8.4	6.3	5.4	6.9	11.4
R_{work} (%)[h]	23.6	24.0	23.8	22.3	23.2
R_{free} (%)[h]	26.6	26.7	27.9	28.9	28.7
No. of residues					
Protein	476	476	476	476	476
Solvent atoms	95	95	38	31	4
Ions	0	0	1	2	1
Ribonucleotides	9	11	11	9	12
RMS deviation from ideal geometry					
Bond lengths (Å)	0.006	0.002	0.001	0.009	0.003
Bond angles (°)	0.8	0.5	0.4	0.9	0.6
Avg temp factors (Å)					
Protein	49.9	47.2	34.2	25.2	55.4
Solvent and ions	54.2	55.2	49.5	27.7	54.2
Ribonucleotides	80.2	78.7	76.1	50.0	88.8

[a] PDB code 3KMS.
[b] PDB code 3KMQ.
[c] PDB code 3KNA.
[d] PDB code 3KOA.
[e] PDB code 3KLV.
[f] Di, intensity divided by its standard definition (I/σ).
[g] $R_{merge} = \Sigma_j\Sigma_h (|I_jh - \langle I_h\rangle|)/\Sigma_j\Sigma_h(\langle I_h\rangle)$, where h is a unique reflection indice, I_jh are the intensities of symmetry-related reflections, and $\langle I_h\rangle$ is the mean intensity.
[h] R_{work} and R_{free} are defined by $R = \Sigma_{hkl}||F_{obs}| - |F_{calc}||/\Sigma_{hkl}|F_{obs}|$, where h, k, and l are the indices of the reflections (used in refinement for R_{work}; 5%, not used in refinement, for R_{free}) and F_{obs} and F_{calc} are the structure factors deduced from measured intensities and calculated from the model, respectively.

3D(G62S-M296I) are available at the Protein Data Bank (PDB entries 3KNA, 3KOA, 3KMS, 3KMQ, and 3KLV, respectively).

RESULTS

Instability of FMDV encoding 3D with G62S is compensated for by the 3D replacement M296I. Contrary to PV, an FMDV with the replacement G62S in 3D was never selected in the presence of R (1, 28). There are at least four possible interpretations of this result: (i) G62S does not confer any resistance to R, (ii) it inflicts too great a fitness cost upon FMDV, (iii) the requirement of at least two mutations (one transition and one transversion or two transversions) is too high a genetic barrier for the substitution to occur, or (iv) a combination of these possibilities. To approach this question, mutant FMDVs expressing 3D with G62S, M296I, or both substitutions were constructed in the sequence context of the parental reference FMDV C-S8c1 as detailed in Materials and Methods. Previously, we showed that pMT28-3D(M296I) was as stable as wild-type pMT28-3D (virus with wild-type 3D) upon passage in the presence or absence of R (28). Here, transcripts from pMT28-3D, pMT28-3D(G62S), and pMT28-3D(G62S-M296I) were transfected into BHK-21 cells in the absence or presence of R and the progeny was subjected to five serial passages in BHK-21 cells, also in the absence or presence of R. Passages were carried out in triplicate, and the 3D coding regions of the initial progeny obtained upon transfection and samples from subsequent passages were sequenced. The results (Fig. 1A) documented the high genetic instability of FMDV pMT28-3D(G62S), which reverted completely to wild-type 3D in two out of the three parallel lineages. Additional studies are needed to clarify why FMDV with G62S in 3D remained stable in one of the three lineages, since no other mutations were detected in the 3D coding region. The viral population of the lineage that maintained G62S in 3D was used for additional biological experiments. In contrast, pMT28-3D(G62S) remained stable (or with dominance of the substituted residue) in the presence of R. pMT28-3D(G62S-M296I) displayed genetic stability in the absence and presence of R. The results suggest that the presence of the 3D replacement G62S inflicts a selective disadvantage on FMDV that is partially compensated for by the presence of M296I in the same molecule.

In standard infections in liquid culture medium, the presence of G62S in 3D decreased the production of infectious progeny and the sensitivity to R (Fig. 1B and C). To confirm that G62S in 3D decreased FMDV fitness in the presence of M296I, pMT28-3D(G62S-M296I) was competed with an equal number of PFU of either pMT28 or pMT28-3D(M296I). In both cases, virus with S62 was rapidly outcompeted by virus with G62 [>80% dominance of G62 in the competition against pMT28 and >60% in the competition against pMT28-3D(M296I) after a single passage at a final multiplicity of infection of 0.1 PFU/cell, as deduced from the relative abundance of each nucleotide in the sequencing band pattern (data not shown)]. Thus, the results of RNA transfection and of infectious progeny production suggest that although M296I exerts some compensatory effect on G62S in 3D, this compensation is not sufficient for the virus to reach the replicative efficacy of wild-type FMDV.

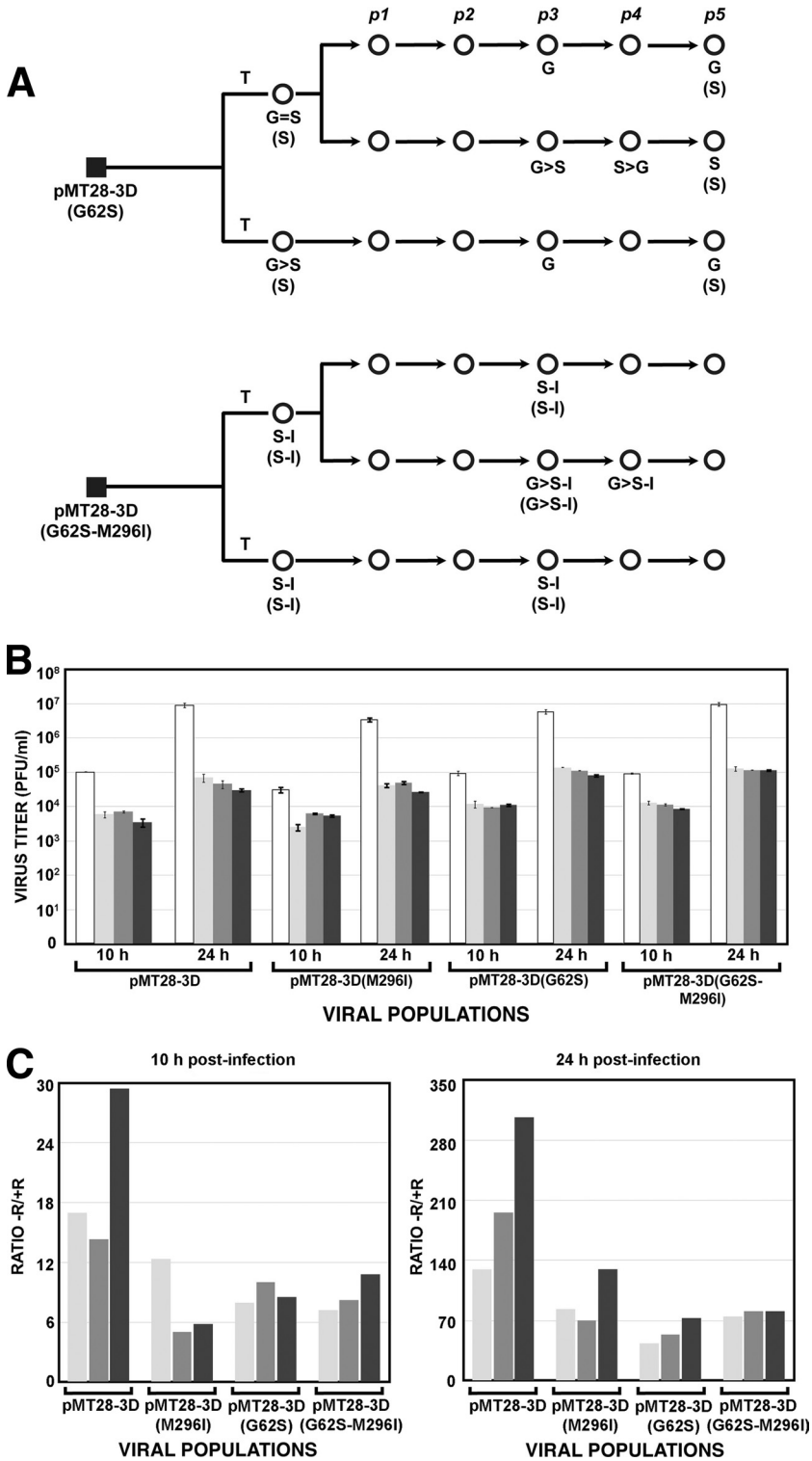

FIG. 1. Behavior of FMDV mutants with the replacements G62S and M296I in 3D. (A) Scheme of the passages of pMT28-3D(G62S) and pMT28-3D(G62S-M296I) in BHK-21 cells. Filled squares represent the initial RNA transcript used for two transfections (T). Progeny viral populations are depicted as filled squares, and the letter *p* stands for passage number. Passages were carried out in the absence or presence of R, as explained in the text. Below each viral population, the dominant amino acids at positions 62 (G or S) and 296 (M or I) are indicated (an equality sign indicates equal proportions of the two amino acids, a greater-than sign indicates about 70% of the amino acid written first, and S-I means a double-mutant polymerase with S62 and I296). The mutant dominances upon transfection and passages in the presence of R are given in parentheses. (B) Infectious progeny production by pMT28-3D (wild type) and pMT28 expressing mutant polymerases in the absence (empty bars) or presence of 200, 400, or 800 μM R (increasingly darker gray bars) at 10 and 24 h postinfection. (C) Ratio of infectious progeny production in the absence of R relative to the presence of 200, 400, and 800 μM R (increasingly darker gray bars). Symbols are as in panel B. Procedures are described in Materials and Methods.

The substitution G62S in 3D of FMDV decreases polymerase and RNA-binding activities. To investigate whether the behavior of viruses with G62S and M296I in their 3D was paralleled by differences in the activities of the polymerases, the four enzymes [3D, 3D(G62S), 3D(M296I), and 3D(G62S-M296I)] were purified and compared regarding polymerization activity. The poly(U) synthesis activity of 3D(M296I), using poly(A)-oligo$(dT)_{15}$ as a template-primer, was similar than that of wild-type 3D. However, the polymerases harboring G62S substitution [both 3D(G62S) and 3D(G62S-M296I)] showed a statistically significant reduction of poly(U) synthesis, indicating an adverse effect of G62S during RNA polymerization (Fig. 2A).

To explore whether the reduction in polymerase activity could be due to a defect in RNA binding, the mutant polymerases were subjected to gel mobility shift assays with sym/sub-U RNA. While 3D(M296I) retarded the same amount of RNA as 3D did, both 3D(G62S) and 3D(G62S/M296I) bound a significantly smaller amount of RNA (Fig. 2B). These results are in agreement with the low activity displayed by the polymerases that harbor G62S and may explain the defect in replication exhibited by the corresponding mutant viruses in cell culture in the absence of R.

Mutant polymerases exhibit less incorporation of RMP into RNA than wild-type 3D does. To determine how polymerases 3D, 3D(M296I), 3D(G62S), and 3D(MG62S/M296I) discriminated RTP as a substrate for RNA elongation, relative to the incorporation of GTP or ATP, heteropolymeric sym/sub template-primers were used. The incorporation of either GTP or ATP at position +1 of sym/sub-C or sym/sub-U, respectively, was very fast, with about 30% of the primer elongated during the first 20 s, in agreement with previous results (3) (Fig. 2C and D). For all polymerases, the incorporation of RMP was much slower than that of the correct nucleotide. At 20 min of reaction with sym/sub-C, the ratio of incorporation of GMP relative to RMP was 1.9 for wild-type 3D and 5.2 to 18.9 for the mutant polymerases. The ratios of incorporation of AMP relative to RMP in similar assays carried out with sym/sub-U were 7.3 for wild-type 3D and 16.3 to 20.9 for the mutant enzymes, which are the maximum ratios obtained with the enzymes that included G62S. Thus, the substitution G62S in 3D reduced the capacity to incorporate RMP during RNA synthesis.

The structure of the 3D mutant polymerases in complexes with RNA. To analyze the possible structural changes in the FMDV polymerase associated with the mutations, different 3Ds harboring the M296I, G62S, and M296I-G62S substitutions were crystallized in complex with an heteropolymeric sym/sub-U RNA with the sequence 5′CGAUGGGCCC3′ and analyzed by X-ray diffraction. Two different crystal forms, space groups $P4_12_12$ and $P3_221$, were obtained from the 3D(M296I)-RNA and 3D(G62S)-RNA complexes, whereas only $P3_221$ crystals were obtained from the 3D(G62S-M296I)-RNA double mutant complex (Table 1). The trigonal $P3_221$ crystals of 3D(M296I)-RNA were used to obtain the ternary complex 3D(M296I)-RNA-GTP as described in Materials and Methods. Attempts to obtain other ternary complexes by using M296I, G62S, or G62SM296I mutant complexes in the presence of ATP or RTP were unsuccessful, despite the use of different substrate concentrations and incubation times. The X-ray structures of the different complexes were determined at resolutions ranging from 2.1 to 2.8 Å (Table 1). For all of the structures analyzed, the resulting difference maps allowed unequivocal tracing of the mutated and surrounding residues that were omitted from the initial models to eliminate model bias and showed the presence of the template-primer RNA duplex in the front channel of the polymerase (Fig. 3). The 3D(M296I)-RNA structures showed clear densities to position nucleotides A3 and U4, occupying the template channel of the polymerase as previously described for the wild-type 3D elongation complexes (Fig. 3A and 4A and C) (13). In contrast, the 5′ overhang region of the template chain appeared totally disordered in the 3D(G62S)-RNA and 3D(G62SM296I)-RNA structures. In the 3D(G62SM296I)-RNA complex, the hydroxyl group O2′ of the ribose moiety of G5 interacted tightly with the main-chain nitrogen atoms of amino acids Cys300 and Ser301 of the β9-α11 loop (Fig. 3B). Weak density was seen to accommodate the guanine base, which did not appear Watson-Crick paired with C20. The electron density of nucleotide C20 was sufficiently clear to define its position, with the cytosine base establishing a double hydrogen bond with the side chain of Ser304. In the 3D(G62S)-RNA complex, nucleotide G5 appeared totally disordered, and only density to accommodate the 5′ phosphate was visible (Fig. 3C). Despite the disorder of its pair (G5), the primer nucleotide C20 was visible in the structure, occupying a position similar to that described in previous FMDV 3D structures (Fig. 3C) (13, 14).

The structure of the 3D(M296I)-RNA-GTP complex shows the GMP molecule incorporated into the nascent RNA, occupying the 3′ end of the primer terminus at the active site. Misincorporated guanine base G21 contacts acceptor base U4 of the template, and the double-stranded RNA appears to be elongated by 1 bp (Fig. 3A and 4). The pyrophosphate product was also seen in the ribonucleoside triphosphate (rNTP) entry tunnel, interacting with Lys387 of motif E (Fig. 4C). No major structural changes were observed in the polymerase active site when 3D(M296I)-RNA and 3D(M296I)-RNA-GTP were compared (Fig. 4; see Table S2 in the supplemental material). Only the side chain of Thr303 within loop β9-α11 changed its rotamer conformation after GMP incorporation (Fig. 4C). In the 3D(M296I)-RNA complex, the hydroxyl group of Thr303 side chain was hydrogen bonded to the side chain of Asn307 in motif B. After GMP incorporation, the rotated Thr303 side chain contacted the main-chain nitrogen atom of Cys300 of the same β9-α11 loop. The equivalent local change in the Thr303 side chain was previously observed after the incorporation of the correct nucleotide ATP by the wild-type 3D polymerase, as well as after the incorporation of the 5-fluorouridine triphosphate analogue (13). Superimposition of the 3D-RNA structure on the mutated 3D(M296I)-RNA and 3D(M296I)-RNA-GTP complexes revealed additional conformational changes in the β9-α11 loop. In particular, the mutated polymerase shows a rotation of the peptide bonds Ser298-Gly299 and Cys300-Ser301 (Fig. 4A and B). These residues interact directly with the template acceptor nucleotides in both the M296I-RNA and M296I-RNA-GTP complexes (Fig. 4A and C). The misincorporated GMP base appears hydrogen bonded to the Ser304 side chain. Thus, the presence of M296I in 3D of FMDV results in conformational changes that can influence nucleotide recognition.

As expected, the structures of 3D(G62S)-RNA that crystal-

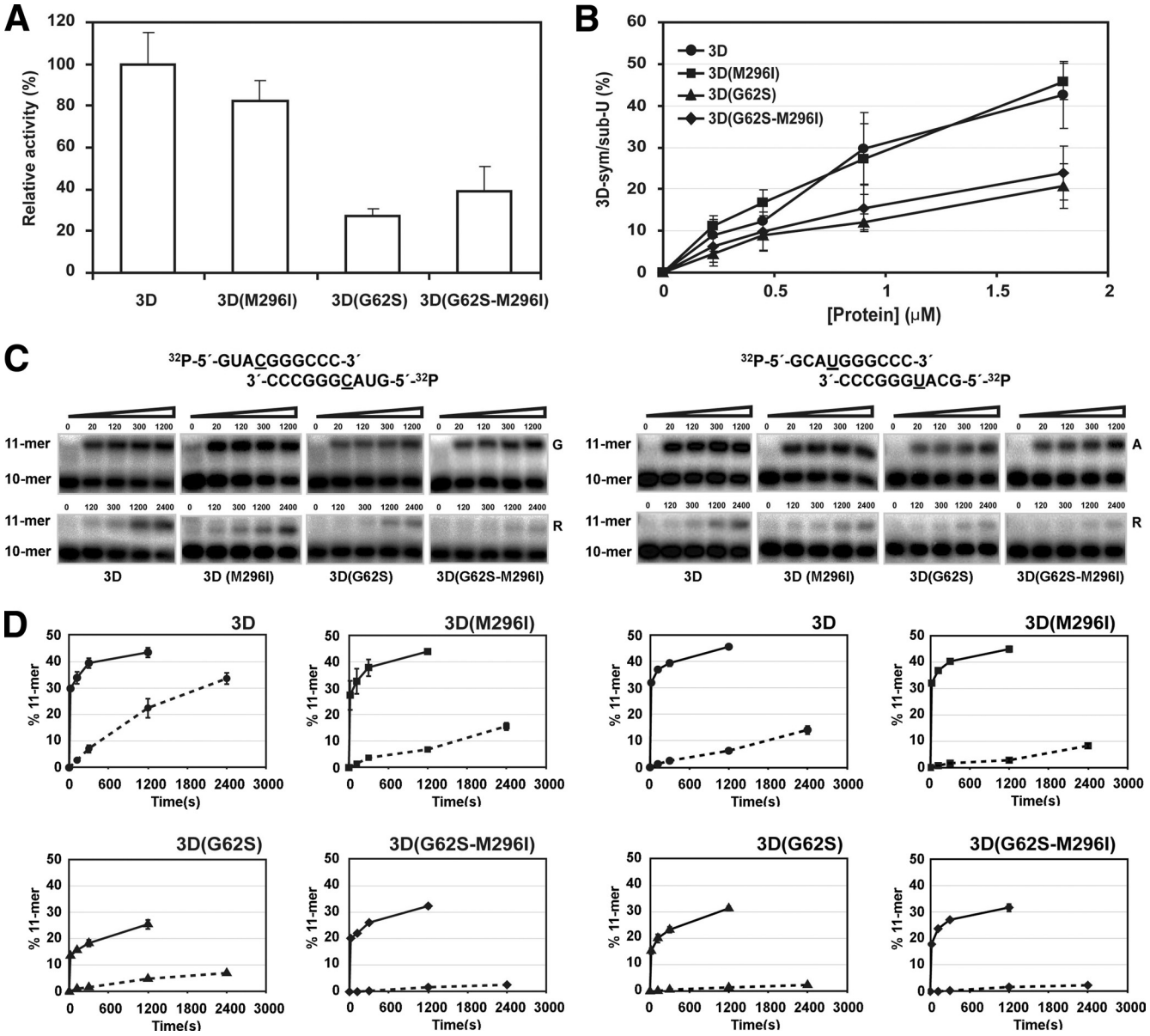

FIG. 2. Polymerization and RNA-binding activities of wild-type and mutant FMDV 3Ds. (A) Incorporation of [α-^{32}P]UTP using poly(A)/oligo(dT)$_{15}$ as a template primer. Values are given relative to that of wild-type 3D. Results are the average of triplicate determinations, and standard deviations are given. The statistical significance of the differences (two-tailed *t* test for independent samples, 4 degrees of freedom, critical *t* value of 2.776, $P = 0.05$) is the following: 3D-3D(M296I), $t = 1.27$, $P > 0.5$; 3D-3D(G62S), $t = 9.37$, $P < 0.001$; 3D-3D(G62S-M296I), $t = 6.48$, $P < 0.005$; 3D(M296I)-3D(G62S), $t = 11.2$, $P < 0.001$; 3D(M296I)-3D(G62S-M296I), $t = 6.52$, $P < 0.005$; 3D(G62S)-3D(G62S-M296I), $t = 2.30$, $P > 0.1$. (B) Binding of wild-type and mutant 3D to sym/sub-U RNA, measured as a percentage of retarded label in a gel mobility shift assay, as a function of protein concentration. The values are averages of three determinations, and standard deviations are given. (C) Electrophoretic analysis of the products that result from the incorporation of either GTP (G) or RTP (R) into sym/sub-C (left panels) and incorporation of either ATP(A) or RTP (R) into sym/sub-U (right panels) catalyzed by the indicated polymerases. (D) Percentage of elongated sym/sub as a function of the time of polymerization reaction by the indicated polymerases. The four panels on the left correspond to incorporation of GTP (solid lines) or RTP (dashed lines) using sym/sub-C as a template-primer. The four panels on the right correspond to the incorporation of ATP (solid lines) or RTP (dashed lines) using sym/sub-U as a template-primer. Protocols for the polymerization assays, mobility shift RNA-binding assay, and electrophoretic analysis of sym/sub RNAs are detailed in Materials and Methods.

lized in tetragonal and trigonal space groups are almost identical. The root mean square (RMS) deviation of the superimposition of all polymerase residues is only 0.27 Å, with the largest deviations concentrated in the solvent-exposed loops that participate in crystal-packing interactions (see Table S2 in the supplemental material). These structures are also similar to that of the 3D(G62S-M296I)-RNA complex, where the only significant rearrangement is an ~2-Å movement of residues from Ser298 to Ala302 (see Table S2 in the supplemental material). The observed structural changes directly affect the interactions with the template acceptor nucleotide (Fig. 3B and C). Furthermore, subtle changes are observed in the re-

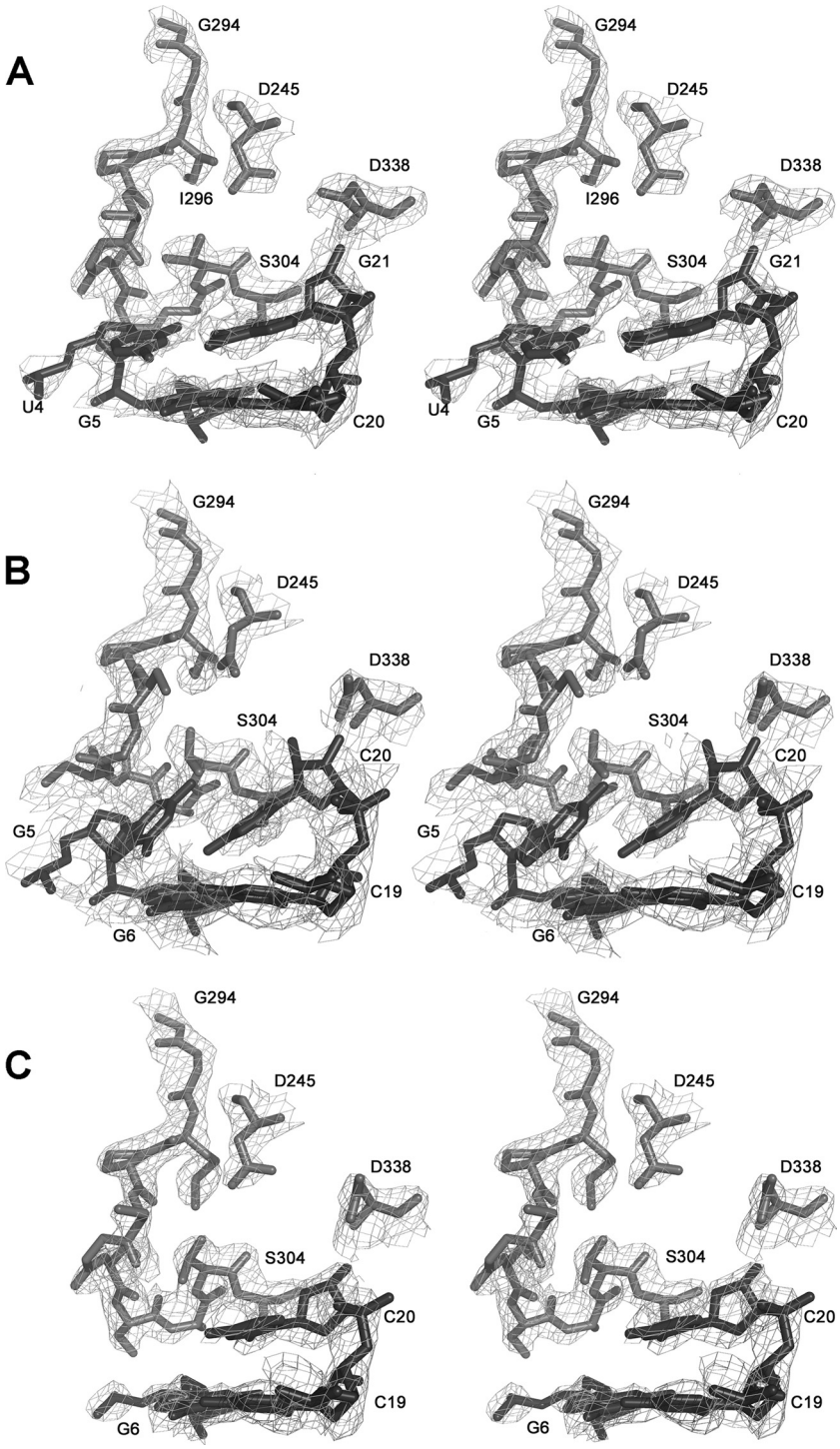

FIG. 3. Structures and interactions at the active site of mutant 3D proteins (A) 3D(M296I)-RNA-GTP, (B) 3D(G62S-M296I)-RNA, and (C) 3D(G62S)-RNA. Shown are stereo views of σ_A-weighted $|F_o|-|F_c|$ electron density maps around the active-site residues of the polymerase that were omitted from the phasing model. The model is placed inside the density in a stick representation. The polymerase residues are shown in gray and explicitly labeled. The first two base pairs of the RNA template-primer are shown in black.

gion around position 62 of the finger domain when the G62S and G62S-M296I structures are compared and when these structures were compared with those of the wild-type polymerase elongation complexes (see Table S2 in the supplemental material). These residues participate in an extensive network of hydrogen bonds that involves the G62 region (from Lys61 to Lys65), the N terminus (from Gly1 to Ile3), the β9-α11 loop (from Gly294 to Ser304), and different residues in conserved motifs A (from Phe244 to His248) and B (Asn307) (Fig. 5). Thus, an extensive network of interactions allows the replace-

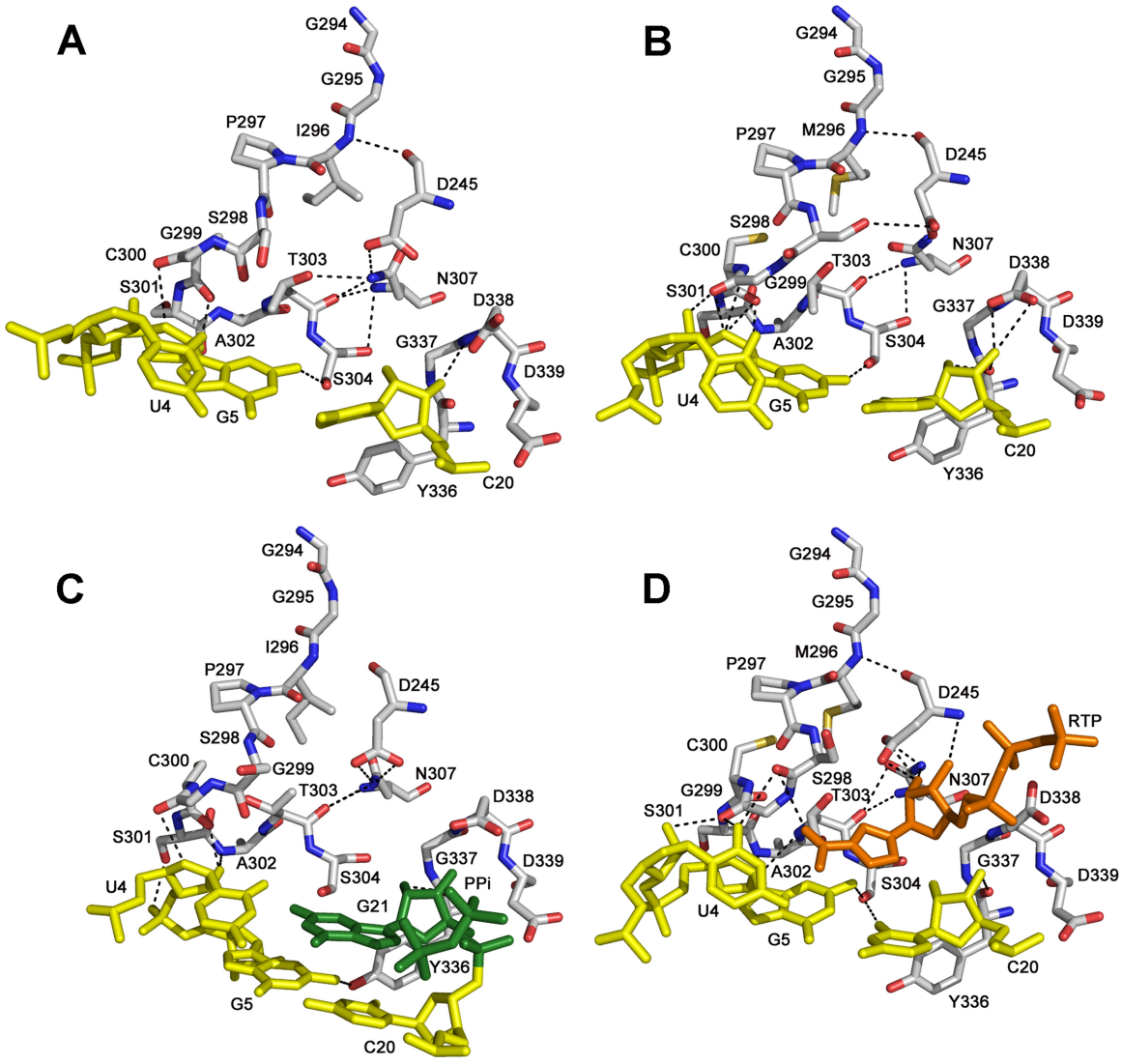

FIG. 4. Structures and interactions in the FMDV 3D active site in different complexes. (A) 3D(M296I)-RNA template-primer, (B) 3D(wild type)-RNA (PDB code 1WNE), (C) 3D(M296I)-RNA-GTP, and (D) 3D(wild type)-RNA-RTP (PDB code 2E9R). The polymerase residues at the active site are shown as sticks in atom type color and explicitly labeled. The RNA template-primers are shown in yellow (only the first base pairs are represented). In panel C, the newly incorporated nucleotide and the PP_i by-product are shown in green. When the RTP molecule (orange) is located at the active site of wild-type 3D (in panel D), the R pseudobase establishes a number of specific contacts with residues Ser298 and Gly299, within the loop β9-α11 of 3D. This β9-α11 loop changes its conformation to accommodate the nucleoside analog in the cavity. The side chains of residues Asp245 of motif A and Asn307 of motif B have also changed their rotamer conformations to facilitate the interactions with the ribose moiety of the mutagenic nucleotide. The substitution M296I seems to prevent the conformational changes in loop β9-α11, as well as the side-chain rearrangements in residues Asp245 and Asn307 required to interact with R.

ment G62S to influence the conformation of loops adjacent to template and nucleotide recognition sites of 3D.

DISCUSSION

Quasispecies dynamics confers a great adaptive potential on RNA viruses that extends to the selection of viral mutants resistant to mutagenic agents that can jeopardize the efficacy of antiviral treatments based on lethal mutagenesis (22; review in reference 10). Two seemingly unrelated substitutions in picornavirus 3Ds (G64S in PV and M296I in FMDV) were selected to decrease virus sensitivity to R. Reconstruction of FMDV with G62S (equivalent to G64S in PV) has documented the genetic instability of the virus, which explains the absence of this mutation in mutant spectra of FMDV, including components of mutant spectra of populations passaged in the presence of low or high R concentrations (1, 22, 28). In two out of three evolutionary lineages, two transversions occurred that resulted in reversion of S62 to G62. The ease of occurrence of the double transversion renders it very unlikely that the genetic barrier to the production of the replacement G62S was the main obstacle to this substitution's being selected upon the replication of FMDV in the presence of R. Rather, the main obstacle was probably the deleterious effect of G62S on the RNA-binding and polymerase activities of 3D. The structural studies with substituted polymerases described

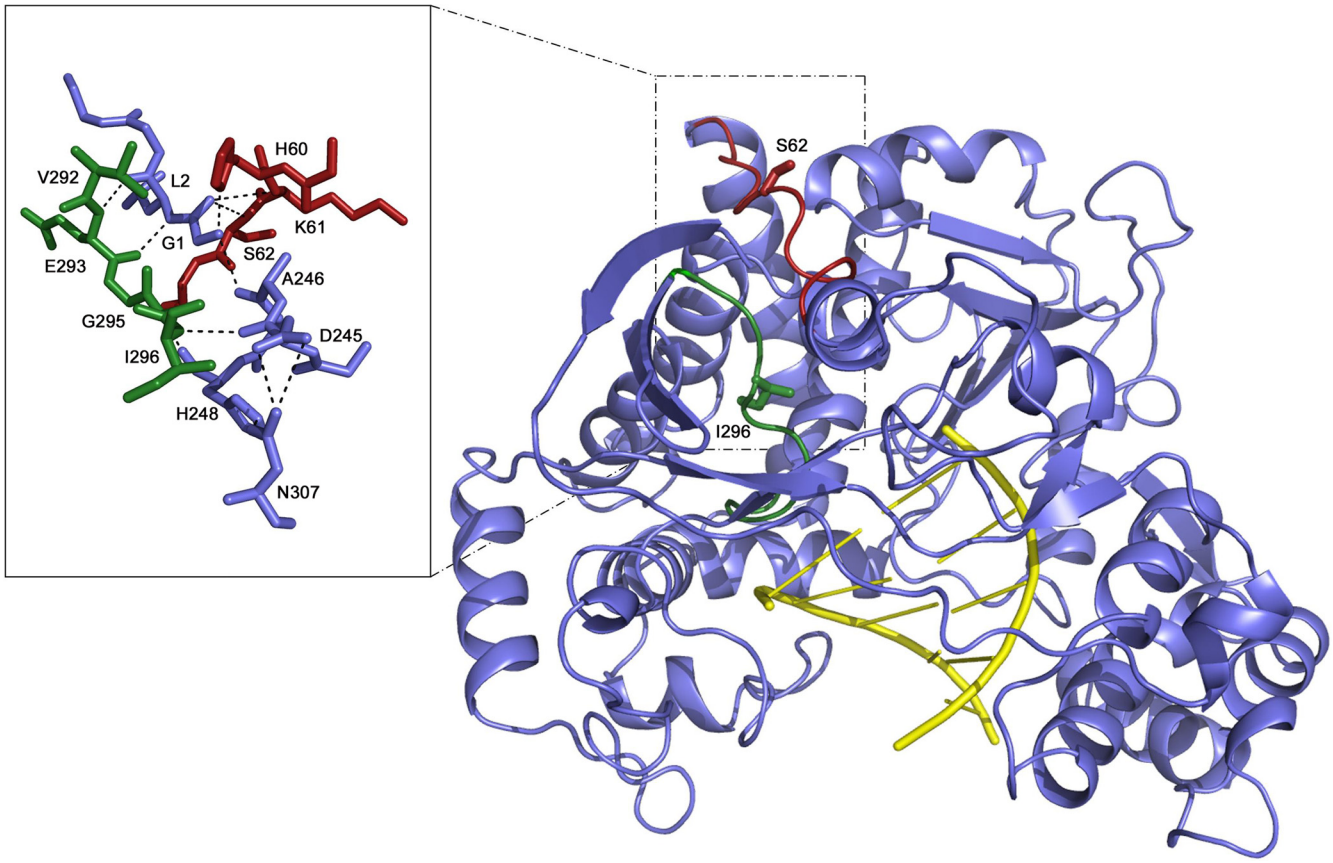

FIG. 5. Top-down view of the structure of the FMDV 3D(G62SM296I)-RNA complex. The polymerase is blue, and the RNA is yellow. Loops α2-α3 and β9-α11, containing the S62 and I296 substitutions, respectively, are red and green with the substituted amino acids represented as balls and explicitly labeled. The right inset shows a close-up of the hydrogen bonding network connecting the G62 region, the polymerase N terminus, the β9-α11 loop, and the active site.

here provide a molecular interpretation of the instability of FMDV harboring G62S in 3D and of the R resistance conferred by M296I and G62S.

Resistance to R conferred by M296I involves steric hindrance. The crystal structure of the FMDV 3D-RNA-RTP complex determined previously revealed that the mutagenic nucleoside was positioned at the active site of the polymerase, adjacent to the 3′ terminus of the primer, and base paired with the acceptor base U4 of the template strand (13). When RTP occupied the nucleotide binding site, the R pseudobase established a number of specific interactions with the main chain of residues Ser298 and Gly299 in loop β9-α11. These residues moved about 2 Å from their position in the unbound form, favoring the accommodation of the pseudobase, as well as the contacts with the template acceptor nucleotide U4 (Fig. 4D). Asp245 and Asn307 also changed their conformation to optimize the interaction with the O2′ hydroxyl group of the ribose moiety, which is located at the active site in the correct position for catalysis. At this position, the side chain of Asp245 forms van der Waals contacts with the Met296 side chain (distance from Met296 Cβ to Cγ Asp245 of 4 Å and from Cβ to Oδ1 of 3.1 Å [13]). Since crystals of the 3D(M296I)-RNA-RTP complex could not be obtained, a model of RTP binding to this mutant form was built based on the structure of the RTP complex obtained for wild-type polymerase (13). The resulting model shows that the M296I mutant form would not adopt the closed conformation required for a wild-type polymerase to interact with RTP through this loop. When an Ile residue occupied position 296, the side chain of Asp245 was not able to reach the expected position to specifically interact with RTP due to a steric conflict with the Cγ2 atom of the Ile side chain (Fig. 6). Antiviral resistance involving steric hindrance with β-branched amino acids was previously described in the HIV-1 and hepatitis B virus reverse transcriptases (8, 27). Finally, the conformation changes in the β9-α11 loop induced in the wild-type polymerase by R binding are not observed in any of the 3D(M296I) structures determined.

In contrast to the restrictions observed in the structure of the 3D(M296I) mutant in RTP incorporation, this mutant was able to misincorporate GMP into the nascent RNA, as shown in the structure of the 3D(M296I)-RNA-GTP elongation complex (Fig. 4C). The structural results suggest that the positioning and interactions of RTP at the polymerase active site are different than the positioning and interactions of natural rNTP substrates. The structure of one wild-type 3D elongation complex with natural substrates is actually available, that of 3D-RNA-ATP/UTP, where the ATP molecule was incorporated into the nascent RNA and the UTP was located close to the

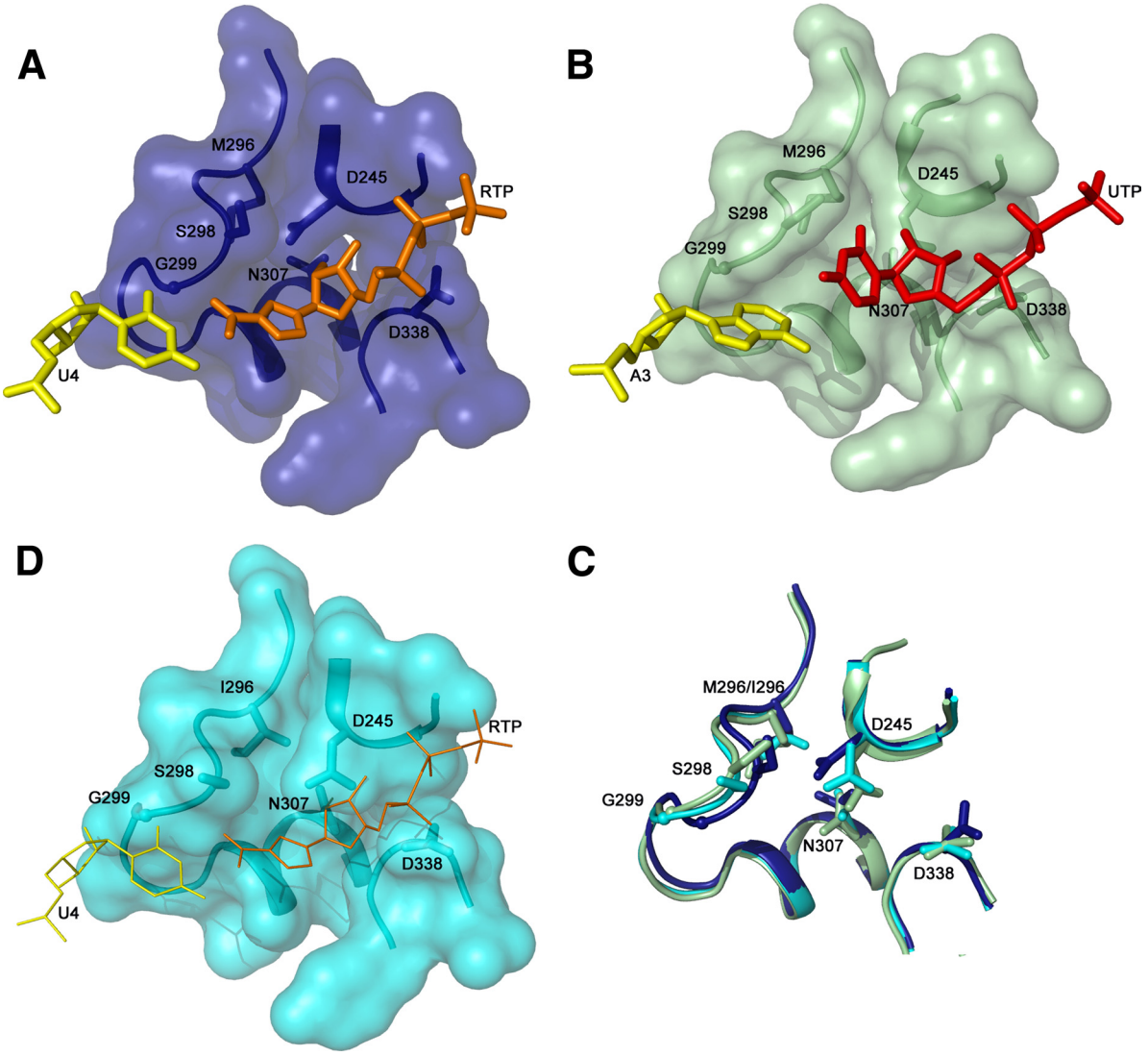

FIG. 6. Surface representation of the active site of the FMDV 3D polymerase. Loop β9-α11 and the regions containing Asp245 (site A), Asn307 (site B), and Asp338 (site C) are shown for the different structures. (A) 3D(wild type)-RNA-RTP with the polymerase residues represented in blue and the template nucleotide U4 and the RTP molecule in yellow and red, respectively. (B) 3D(wild type)-RNA-ATP/UTP with the polymerase residues shown in light green and the template and incoming nucleotides in yellow and red, respectively. (C) 3D(M96I)-RNA with the polymerase residues shown in cyan. The RTP molecule (thin sticks in red) is modeled into the cavity to illustrate the steric impediment between the side chain of Asp245 and the RTP sugar moiety. (D) Structural superimposition of loop β9-α11 and the active-site residues in the three different structures, 3D(wild type)-RNA-RTP (dark blue), 3D(wild type)-RNA-ATP/UTP (light green), and 3D(M96I)-RNA (cyan).

active site (13). Comparisons of 3D-RNA-RTP and 3D-RNA-ATP/UTP showed a number of changes at the active site of 3D. In the presence of RTP, the β9-α11 loop acquired a closed conformation that approached the R pseudobase, allowing the interactions described above that would help the accommodation of RTP at the active site (Fig. 4C and 6A). In the 3D-RNA-ATP/UTP complex, the β9-α11 loop acquired a more open conformation, leaving enough room for the positioning of the A · U pair (Fig. 6B). This open conformation seems also to be required to accommodate the other natural base pairs, C · G, G · C, and U · A, at the active site. The side-chain conformations of Asp245, Asn307, and Asp338 were also different in the different structures. Unfortunately, in the 3D-RNA-ATP/UTP structure, the UTP molecule was not totally positioned at the active site to form a Watson-Crick pair with the adenine acceptor base of the template and the precise interactions which stabilize the UTP substrate in the correct conformation for the catalysis were not established at all.

Taking together all of the data, we conclude that the substitution M296I seems to prevent the conformation rearrangements in loop β9-α11 and Asp245 required to specifically interact with R and that these changes are not needed to interact with natural substrates. These structural results provide an interpretation of the decreased capacity of 3D(M296I) to incorporate RTP relative to that of the wild-type enzyme (28) and are in accordance with previous kinetic data on correct and incorrect nucleotide incorporation by 3D and 3D(M296I) (3).

The G62S and G62S-M296I substitutions. Amino acid 62 in FMDV 3D is located in an exposed region of the finger subdomain, within the loop connecting helices α2 and α3, at 13.1 Å of residue 296 (Cα-Cα distance), which is close to the active site (Fig. 5). However, amino acid 62 and surrounding residues participate in an extensive network of interactions involving the N terminus of 3D, loop β9-α11, and active-site residue Asp245 (Fig. 5). In PV, the equivalent mutation G64S resulted in a polymerase with increased fidelity, allowing the polymerase to discriminate against incorrect nucleotides and RTP. The lower overall rate of spontaneous mutation in the virus comes at the expense of making 3D less efficient at nucleotide incorporation. The structure of native PV 3D showed that G64 is involved in a network of interactions (31) similar to those observed with FMDV 3D (see Fig. S7 in the supplemental material). The crystal structure of PV 3D with the substitution G64S was also determined, and the mutant enzyme displayed a conformation similar to that of the wild-type enzyme (18). The arrangement of residues involved in the hydrogen-bonding network noted for FMDV 3D were also similar, except that the side chain of S64 formed additional hydrogen bonds in PV 3D (18) (see Fig. S7 in the supplemental material). Since no large rearrangements were evident in mutant PV 3D relative to wild-type 3D, the authors hypothesized that the mutation affected fidelity and efficiency primarily by helping to lock the polymerase N terminus and its surroundings in a more rigid arrangement. A similar situation is found when the structures of the FMDV 3D and 3D(G62S) polymerases are compared. However, the structures of PV were obtained in the absence of any RNA template-primer and the changes observed in the β9-α11 loop of FMDV 3D were not detected in the equivalent loop of PV. In FMDV, residues K61 and G62/S62 directly contact Gly1 at the 3D N terminus and amino acids Gly1 and Leu2 are hydrogen bonded with residues Ala246 of motif A and Val292 and Glu293, close to loop β9-α11. In addition, the main chain of residues His248 and Asp245 of motif A are hydrogen bonded to the main chain of Gly295 and Met296 within loop β9-α11 (Fig. 5; see Fig. S7 in the supplemental material). The local perturbation introduced by the replacement of residue G62 with more rigid residue S62 appears to affect the flexibility of loop β9-α11, resulting in a more rigid active site of the polymerase with a reduced ability to interact with the template nucleotides. The structure of the 3DG62S-RNA complex does not show any interaction between loop β9-α11 and the template acceptor nucleotide, which appears mostly disordered (Fig. 3C). The structure of 3D(G62S-M296I) revealed a conformational change in β9-α11 and a number of interactions between residues Ser301 and Ala302 of this loop and the template acceptor nucleotide, despite the absence of an incoming nucleotide at the active site (Fig. 3B). However, the loop did not attain the conformation of wild-type 3D, a fact that could account for suboptimal RNA synthesis by 3D(G62S-M296I) and the selective disadvantage of FMDV with the two replacements relative to FMDV with only M296I. That M296I failed to restore the functionality of the wild-type active site is also suggested by the decreased RNA-binding activity of 3D(G62S-M296I), which resembles the binding activity of 3D(G62S) rather than that of 3D(M296I) (Fig. 2).

From the structural results, we conclude that although G62 and M296 are separated by more than 13 Å, the loops containing these substitutions are tightly connected through an extensive network of interactions that involve residues around G62, the β9-α11 loop, and the active site of the enzyme. Thus, the small perturbations observed in the loop containing residue 62 might be transmitted to the active site via hydrogen bonds. Despite the clear negative effects of G62S on the RNA-binding and polymerization activities of 3D, the possibility cannot be excluded that the instability of FMDV with G62S in 3D may also impair other functions that involve 3D or its precursors 3CD and 3ABCD.

The role of the β9-α11 loop in correct and incorrect nucleotide incorporation and R resistance. Previous structural studies of replicative complexes of the wild-type FMDV 3D polymerase revealed no major domain movements either upon RNA binding or upon rNTP incorporation (13). A similar observation has been made here with the structural analyses of the replicative complexes of polymerases with the substitutions G62S and M296I. The structural superimpositions of all of the elongation complexes show RMS deviations ranging from 0.25 to 0.56 Å, with the largest deviations located in the β9-α11 loop (see Table S2 in the supplemental material).

In addition to the main-chain changes, a number of side-chain rearrangements are observed at the active site. In particular, Asp245 of motif A changes its side-chain conformer when the incoming rNTP is positioned at the nucleotide binding site. The side chain of Thr303 of the β9-α11 loop changes its conformation once a new nucleotide is incorporated into the nascent RNA. Also, the side chain of Asn307 (motif B) establishes contacts with Asp245 and Thr303 prior to nucleotide incorporation and it changes its conformation upon rNTP binding and incorporation (Fig. 4). It has been demonstrated that picornavirus polymerases require repositioning of Asp245 and Asn307 (amino acid numbers correspond to those of FMDV 3D) to accommodate the incoming nucleotide substrate (5, 16, 19). Asp245 permits communication between the ribose-binding pocket and the catalytic center of 3D. All nucleotide and nucleoside analogues bind the polymerase in a similar ground state configuration via the metal-bound triphosphate residue of the incoming nucleotide. In this configuration, the ribose moiety cannot reach the catalytic site since the Asp245-Asn307 interaction occludes the ribose site. A conformational change occurs, permitting suitable base pairing between the nucleotide and template and the subsequent phosphoryl transfer. The structures of the different 3D elongation complexes determined in this work and in a previous study (14) show that the side-chain rearrangements of Asp245 and Asn307 occur in coordination with the conformational changes of loop β9-α11 in response to the incoming nucleotide. Thus, the polymerase mutations that directly or indirectly affect the β9-α11 loop would, as a consequence, affect nucleotide recognition.

We are currently functionally and structurally studying additional FMDV mutants that have been selected in the presence of R. Such analyses of polymerase replication complexes of mutated polymerases with the ability to evade the antiviral activity of R or other nucleoside analogues should contribute to the understanding of the mechanism of action of this antiviral agent and should facilitate the development of new and more effective antiviral nucleosides.

ACKNOWLEDGMENTS

Work in Barcelona was supported by grant BIO2008-02556, and work in Madrid was supported by grant BFU2008-02816/BMC from MCINN and by Fundación R. Areces. CIBERehd (Centro de Investigación Biomédica en Red de Enfermedades Hepáticas y Digestivas) is funded by Instituto de Salud Carlos III. Work in Barcelona and Madrid was further supported by Proyecto Intramural de Frontera 2000820FO191 (CSIC). X-ray data were collected at ESRF beamlines ID14.1 and ID14.2 (Grenoble, France) within a Block Allocation Group (BAG Barcelona). Financial support was provided by the ESRF. A.A. and C.F.-O. are recipients of I3P and Juan de la Cierva postdoctoral contracts, respectively.

REFERENCES

1. **Airaksinen, A., N. Pariente, L. Menendez-Arias, and E. Domingo.** 2003. Curing of foot-and-mouth disease virus from persistently infected cells by ribavirin involves enhanced mutagenesis. Virology **311:**339–349.
2. **Arias, A., R. Agudo, C. Ferrer-Orta, R. Perez-Luque, A. Airaksinen, E. Brocchi, E. Domingo, N. Verdaguer, and C. Escarmís.** 2005. Mutant viral polymerase in the transition of virus to error catastrophe identifies a critical site for RNA binding. J. Mol. Biol. **353:**1021–1032.
3. **Arias, A., J. J. Arnold, M. Sierra, E. D. Smidansky, E. Domingo, and C. E. Cameron.** 2008. Determinants of RNA-dependent RNA polymerase (in)fidelity revealed by kinetic analysis of the polymerase encoded by a foot-and-mouth disease virus mutant with reduced sensitivity to ribavirin. J. Virol. **82:**12346–12355.
4. **Arnold, J. J., and C. E. Cameron.** 2000. Poliovirus RNA-dependent RNA polymerase (3D(pol)). Assembly of stable, elongation-competent complexes by using a symmetrical primer-template substrate (sym/sub). J. Biol. Chem. **275:**5329–5336.
5. **Arnold, J. J., and C. E. Cameron.** 2004. Poliovirus RNA-dependent RNA polymerase (3Dpol): pre-steady-state kinetic analysis of ribonucleotide incorporation in the presence of Mg2+. Biochemistry **43:**5126–5137.
6. **Crotty, S., C. E. Cameron, and R. Andino.** 2001. RNA virus error catastrophe: direct molecular test by using ribavirin. Proc. Natl. Acad. Sci. U. S. A. **98:**6895–6900.
7. **Crotty, S., D. Maag, J. J. Arnold, W. Zhong, J. Y. Lau, Z. Hong, R. Andino, and C. E. Cameron.** 2000. The broad-spectrum antiviral ribonucleoside ribavirin is an RNA virus mutagen. Nat. Med. **6:**1375–1379.
8. **Das, K., X. Xiong, H. Yang, C. E. Westland, C. S. Gibbs, S. G. Sarafianos, and E. Arnold.** 2001. Molecular modeling and biochemical characterization reveal the mechanism of hepatitis B virus polymerase resistance to lamivudine (3TC) and emtricitabine (FTC). J. Virol. **75:**4771–4779.
9. **Domingo, E., C. Escarmís, E. Lazaro, and S. C. Manrubia.** 2005. Quasispecies dynamics and RNA virus extinction. Virus Res. **107:**129–139.
10. **Domingo, E., C. Escarmís, L. Menéndez-Arias, C. Perales, M. Herrera, I. S. Novella, and J. J. Holland.** 2008. Viral quasispecies: dynamics, interactions, and pathogenesis, p. 87–118. *In* E. Domingo, R. Parrish, and J. J. Holland (ed.), Origin and evolution of viruses. Elsevier, Oxford, United Kingdom.
11. **Emsley, P., and K. Cowtan.** 2004. Coot: model-building tools for molecular graphics. Acta Crystallogr. D Biol. Crystallogr. **60:**2126–2132.
12. **Escarmís, C., M. Davila, N. Charpentier, A. Bracho, A. Moya, and E. Domingo.** 1996. Genetic lesions associated with Muller's ratchet in an RNA virus. J. Mol. Biol. **264:**255–267.
13. **Ferrer-Orta, C., A. Arias, R. Perez-Luque, C. Escarmís, E. Domingo, and N. Verdaguer.** 2007. Sequential structures provide insights into the fidelity of RNA replication. Proc. Natl. Acad. Sci. U. S. A. **104:**9463–9468.
14. **Ferrer-Orta, C., A. Arias, R. Perez-Luque, C. Escarmís, E. Domingo, and N. Verdaguer.** 2004. Structure of foot-and-mouth disease virus RNA-dependent RNA polymerase and its complex with a template-primer RNA. J. Biol. Chem. **279:**47212–47221.
15. **García-Arriaza, J., S. C. Manrubia, M. Toja, E. Domingo, and C. Escarmís.** 2004. Evolutionary transition toward defective RNAs that are infectious by complementation. J. Virol. **78:**11678–11685.
16. **Gohara, D. W., J. J. Arnold, and C. E. Cameron.** 2004. Poliovirus RNA-dependent RNA polymerase (3Dpol): kinetic, thermodynamic, and structural analysis of ribonucleotide selection. Biochemistry **43:**5149–5158.
17. **Graci, J. D., and C. E. Cameron.** 2006. Mechanisms of action of ribavirin against distinct viruses. Rev. Med. Virol. **16:**37–48.
18. **Marcotte, L. L., A. B. Wass, D. W. Gohara, H. B. Pathak, J. J. Arnold, D. J. Filman, C. E. Cameron, and J. M. Hogle.** 2007. Crystal structure of poliovirus 3CD protein: virally encoded protease and precursor to the RNA-dependent RNA polymerase. J. Virol. **81:**3583–3596.
19. **Ng, K. K., J. J. Arnold, and C. E. Cameron.** 2008. Structure-function relationships among RNA-dependent RNA polymerases. Curr. Top. Microbiol. Immunol. **320:**137–156.
20. **Otwinowski, Z., and W. Minor.** 1997. Processing X-ray diffraction data collected in oscillation model. Methods Enzymol. **276:**307–326.
21. **Parker, W. B.** 2005. Metabolism and antiviral activity of ribavirin. Virus Res. **107:**165–171.
22. **Perales, C., R. Agudo, and E. Domingo.** 2009. Counteracting quasispecies adaptability: extinction of a ribavirin-resistant virus mutant by an alternative mutagenic treatment. PLoS One **4:**e5554.
23. **Perelson, A. S., and T. J. Layden.** 2007. Ribavirin: is it a mutagen for hepatitis C virus? Gastroenterology **132:**2050–2052.
24. **Pfeiffer, J. K., and K. Kirkegaard.** 2005. Increased fidelity reduces poliovirus fitness and virulence under selective pressure in mice. PLoS Pathog. **1:**e11.
25. **Pfeiffer, J. K., and K. Kirkegaard.** 2003. A single mutation in poliovirus RNA-dependent RNA polymerase confers resistance to mutagenic nucleotide analogs via increased fidelity. Proc. Natl. Acad. Sci. U. S. A. **100:**7289–7294.
26. **Roussel, A., and C. Cambilleau.** 1989. Turbo-Frodo. Silicon Graphics, Mountain View, CA.
27. **Sarafianos, S. G., K. Das, A. D. Clark, Jr., J. Ding, P. L. Boyer, S. H. Hughes, and E. Arnold.** 1999. Lamivudine (3TC) resistance in HIV-1 reverse transcriptase involves steric hindrance with beta-branched amino acids. Proc. Natl. Acad. Sci. U. S. A. **96:**10027–10032.
28. **Sierra, M., A. Airaksinen, C. Gonzalez-Lopez, R. Agudo, A. Arias, and E. Domingo.** 2007. Foot-and-mouth disease virus mutant with decreased sensitivity to ribavirin: implications for error catastrophe. J. Virol. **81:**2012–2024.
29. **Sierra, S., M. Davila, P. R. Lowenstein, and E. Domingo.** 2000. Response of foot-and-mouth disease virus to increased mutagenesis: influence of viral load and fitness in loss of infectivity. J. Virol. **74:**8316–8323.
30. **Sobrino, F., M. Davila, J. Ortin, and E. Domingo.** 1983. Multiple genetic variants arise in the course of replication of foot-and-mouth disease virus in cell culture. Virology **128:**310–318.
31. **Thompson, A. A., and O. B. Peersen.** 2004. Structural basis for proteolysis-dependent activation of the poliovirus RNA-dependent RNA polymerase. EMBO J. **23:**3462–3471.
32. **Vignuzzi, M., J. K. Stone, J. J. Arnold, C. E. Cameron, and R. Andino.** 2006. Quasispecies diversity determines pathogenesis through cooperative interactions in a viral population. Nature **439:**344–348.
33. **Vo, N. V., K. C. Young, and M. M. Lai.** 2003. Mutagenic and inhibitory effects of ribavirin on hepatitis C virus RNA polymerase. Biochemistry **42:**10462–10471.